

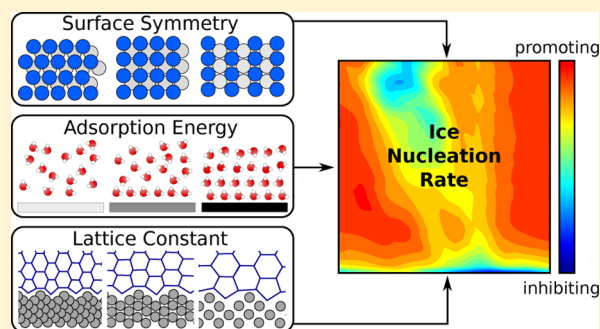
The Many Faces of Heterogeneous Ice Nucleation: Interplay Between Surface Morphology and Hydrophobicity

Martin Fitzner, Gabriele C. Sosso, Stephen J. Cox, and Angelos Michaelides*

London Centre for Nanotechnology, Department of Chemistry and Thomas Young Centre, University College London, 17-19 Gordon Street, London WC1H 0AJ, United Kingdom

S Supporting Information

ABSTRACT: What makes a material a good ice nucleating agent? Despite the importance of heterogeneous ice nucleation to a variety of fields, from cloud science to microbiology, major gaps in our understanding of this ubiquitous process still prevent us from answering this question. In this work, we have examined the ability of generic crystalline substrates to promote ice nucleation as a function of the hydrophobicity and the morphology of the surface. Nucleation rates have been obtained by brute-force molecular dynamics simulations of coarse-grained water on top of different surfaces of a model fcc crystal, varying the water–surface interaction and the surface lattice parameter. It turns out that the lattice mismatch of the surface with respect to ice, customarily regarded as the most important requirement for a good ice nucleating agent, is at most desirable but not a requirement. On the other hand, the balance between the morphology of the surface and its hydrophobicity can significantly alter the ice nucleation rate and can also lead to the formation of up to three different faces of ice on the same substrate. We have pinpointed three circumstances where heterogeneous ice nucleation can be promoted by the crystalline surface: (i) the formation of a water overlayer that acts as an in-plane template; (ii) the emergence of a contact layer buckled in an ice-like manner; and (iii) nucleation on compact surfaces with very high interaction strength. We hope that this extensive systematic study will foster future experimental work aimed at testing the physicochemical understanding presented herein.



1. INTRODUCTION

The formation of ice influences our everyday experience as well as a variety of scenarios, ranging from global phenomena like climate change^{1,2} to processes happening at the nanoscale, like intracellular freezing.^{3,4} It is surprisingly difficult to observe ice crystallization from pure supercooled water, because the pure liquid can be cooled to -40 °C without freezing.^{1,5} In fact, ice nucleation in nature happens mostly thanks to the presence of foreign particles,⁶ ranging from biological compounds to crystalline surfaces.¹ Such spectacular diversity calls for an obvious question: What is it that makes a material a good ice nucleating agent (INA)? The vast body of experimental and theoretical work undertaken within the last few decades in order to answer this seemingly trivial query proves that our understanding of heterogeneous ice nucleation is far from satisfactory.

Recently, a number of excellent experimental works have succeeded in determining which materials can effectively promote heterogeneous ice nucleation, mostly by measuring ice nucleation temperatures or rates, see e.g., refs 7–18. By doing so, the ice nucleating abilities of a large variety of materials have been characterized.^{1,19} This knowledge can for instance be used to decipher and explain the different contributions to ice nucleation in the atmosphere.^{20–24} However, experiments currently do not provide information

into the molecular details of individual ice nucleation events. Because of the length scale involved (nm), insights into the nucleation process can be obtained instead from computer simulations. And indeed, in the past few years a handful of computational studies have been successful in simulating heterogeneous ice nucleation.^{25–37} This indicates that the time is now ripe for furthering our understanding of the microscopic factors that make a material a good INA. Nevertheless, even being able to explore heterogeneous ice nucleation with simulation approaches may not be enough to understand a priori whether and why a material will be a good INA or not. This is because many different ingredients like the morphology of the surface,^{38–41} its hydrophobicity,^{8,31,37,42} local electric fields,^{12,26,43–45} preferential nucleation sites, or surface roughness^{30,32,46} can simultaneously impact on both the molecular mechanism and the resulting nucleation rate.

The two most discussed “requirements” for an effective INA are perhaps the crystallographic match with respect to bulk ice and the strength of the water–surface interaction. The former was introduced by Turnbull and Vonnegut⁴⁷ in order to characterize the catalytic potential of a surface regarding heterogeneous nucleation. If the atomic arrangements in the

Received: August 18, 2015

Published: October 4, 2015

contact region are similar, a disregistry or lattice mismatch δ between the corresponding surface unit cells can be defined in a simplified manner as

$$\delta = \frac{a_s - a_i}{a_i} \quad (1)$$

where a_s and a_i are the lattice parameters of the surface unit cells of the substrate and a certain face of ice. The idea of a small lattice mismatch δ being at the heart of the INA efficacy dates back to the 1940s, when the ice nucleating capabilities of AgI, featuring only $\delta \approx 2\%$ for the basal face, came to light.^{19,48} Even though both experiments^{7,49} and recent simulations^{33,34} have seriously challenged the validity of this concept and most importantly its generality with respect to other materials,^{39,41} a small lattice mismatch is still considered as the primary attribute of an efficient INA. In the case of bacterial ice nucleating proteins, ice-matching patterns have even been used as an a priori assumption to infer the three-dimensional (3D) structure of the residues from the DNA sequence describing the protein.^{50,51}

Concerning the water–surface interaction, or the hydrophobicity/hydrophilicity of a surface, in the last two decades a number of experimental studies investigating ice formation on soot^{1,21,52–56} have prompted a debate about whether a correlation exists between the hydrophilicity of carbonaceous surfaces and their efficacy as INAs. This is a challenging issue, because in most cases the role of the hydrophobicity cannot be disentangled from the influence of the lattice mismatch and surface morphology. As an example, the oxidation of soot taking place in atmospheric aerosols modifies both the hydrophilicity and the morphology of the particles at the nanoscale.⁵⁷ Furthermore, Lupi and Molinero³¹ found that an increase in hydrophilicity showed adverse effects when it was accomplished by adding OH groups as opposed to just increasing the water–surface interaction strength. And indeed, recent experiments by Whale et al.¹⁸ provide some tentative support for this hypothesis. Cox et al. recently investigated the dependence of the ice nucleation rate as a function of hydrophilicity in the case of model nanoparticles.³⁶ They found a similar interaction range for both a fcc and a graphene-like particle where nucleation is enhanced, leading to a rule-of-thumb for an optimal adsorption strength. They also showed³⁷ how a simple modification of the surface morphology could lead to a significant change of nucleation rates, demonstrating the potential of atomic-scale control of nucleation.

As far as we know, the interplay between the hydrophobicity and morphology of the surface has not been systematically studied at the molecular scale. In this work, we fill this shortfall by investigating ice formation on top of a generic fcc crystal as a function of both the strength of the water–surface interaction and the morphology, taking into account the (111), (100), (110), and (211) surfaces. Strikingly different nucleation scenarios emerge according to the balance between the morphology of the surface and its hydrophobicity, thus demonstrating that the lattice mismatch alone cannot be deemed as the key player in promoting nucleation on crystalline surfaces. In addition, we have found that up to three different faces of ice can nucleate on top of the same surface and that the microscopic motivation at the heart of the heterogeneous nucleation process is not unique, but actually changes according to both the water–surface interaction and the morphology of the surface. We propose three microscopic factors that lead to enhancement of the nucleation rates: (i) the

formation of a water overlayer that acts as an in-plane template; (ii) the emergence of a contact layer buckled in an ice-like manner; and (iii) enhanced nucleation on compact surfaces with very high adsorption energy.

The remainder of this paper is organized as follows: Section 2 describes the computational setup (2.1) together with how we obtained nucleation rates and an assessment of finite-size effects (2.2). In Section 3 we present the nucleation rates for all the different surfaces as a function of adsorption energy and lattice constant. From this data we shall extract and discuss the general trends that emerge (3.1). Section 3.2 presents the three different scenarios we propose as driving forces behind the nucleation promotion. We then discuss further insight and future perspectives for improved heterogeneous ice nucleation simulations and experiments that could test the suggestions made here in Section 3.3. Finally, the key results and observations are summarized in Section 4.

2. METHODS

2.1. System and Computational Methods. We considered slab models of crystalline surfaces covered in a water film (see Figure 1a)

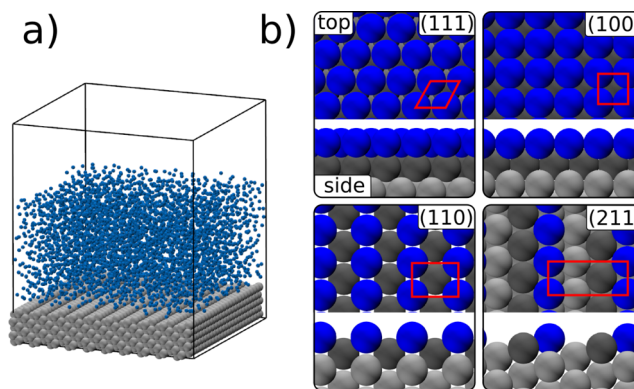


Figure 1. (a) Example of a simulation box used in a heterogeneous ice nucleation run. The coarse-grained water molecules are depicted as blue spheres, while surface atoms are gray. (b) Top and side view of the four crystalline surfaces considered. Atoms are colored according to their z-coordinate. Red boxes highlight the symmetry of the surface unit cells.

including 4000 water molecules represented by the coarse-grained mW model.⁵⁸ This specific water model has excellent structural properties and a melting point close to experiment,⁵⁸ but since it is monatomic it exhibits faster dynamics, which in turn allows for brute-force simulations of nucleation.^{31,32,36,37,59–61} The water film is ~ 35 Å thick, which is enough so that the density is converged to the bulk homogeneous value at ~ 12 Å above the interface.

We remark that in this study we do not aim at investigating specific systems like, e.g., metallic surfaces, but instead we intend to extract general insight and useful trends from idealized model substrates. To this end, we have taken into account four different crystallographic planes of a generic fcc crystal, namely the (111), (100), (110), and (211) surfaces, which exhibit significant differences in terms of atomic roughness and the symmetry of the outer crystalline layer (see Figure 1b). For each of the above-mentioned surfaces, we have built a data set of 10 different slabs varying the fcc lattice parameter a_{fcc} from 3.52 to 4.66 Å.⁶² This range encompasses several fcc metals from Ni to Ag, including the well characterized Pt structure.⁶³ Because of the different surface unit cells and lattice parameters the total simulation box dimensions could not be chosen equal for all simulations. Instead, we employed unit cells as close as possible to the average of $60 \times 60 \times 70$ Å. The interaction of the water with the substrate is given by a truncated Lennard-Jones potential:

$$U(r) = \begin{cases} 4\epsilon \left[\left(\frac{\sigma}{r} \right)^{12} - \left(\frac{\sigma}{r} \right)^6 \right] & r < r_c \\ 0 & r \geq r_c \end{cases} \quad (2)$$

where r is the distance between a water oxygen and a surface atom. The cutoff distance was set to $r_c = 7.53 \text{ \AA}$.

To measure the interaction strength of water with the surface the adsorption energy E_{ads} of a single water molecule was computed. In order to vary this quantity ϵ and σ were changed accordingly. E_{ads} was computed by minimizing the potential energy of a single water molecule on top of the surface. In this manner well-defined adsorption energies can be determined for the (111), (100), and (110) surfaces since only one adsorption site is found by the minimization algorithm. However, for the (211) geometry multiple adsorption sites with considerable energy differences were found.⁶⁴ For this reason we have chosen to assign every ($a_{\text{fcc}}, E_{\text{ads}}$) combination for the (211) orientation the same (ϵ, σ) pair as for the (111) surface. This is also motivated by the (111) terraces exhibited by the (211) surface. The adsorption energy for the (211) geometry as reported in Figure 5 is the arithmetic average of the different adsorption energies found on this particular surface. The averaged results deviate by ca. 5% from those for the (111) surface, e.g., the highest E_{ads} on (111) is around 12.76 kcal/mol, while the average value for the (211) surface with the same (ϵ, σ) parameters is 13.18 kcal/mol. We note that the range of E_{ads} (from 0 to about 13 kcal/mol) we have considered is consistent with typical values obtained by DFT calculations of water monomers on metals.⁶⁵

2.2. Obtaining Nucleation Rates. Heterogeneous ice nucleation events have been simulated by means of brute-force molecular dynamics (MD) simulations, employing the LAMMPS simulation package.⁶⁶ We follow a similar protocol to the one of Cox et al.³⁷ A time step of 10 fs has been used with periodic boundary conditions in the xy -plane while sampling the NVT canonical ensemble with a chain of 10 Nosé–Hoover thermostats^{67,68} with a relaxation time of 0.5 ps. The positions of the surface atoms were fixed throughout the simulations. Every point of the ($a_{\text{fcc}}, E_{\text{ads}}$) grid corresponds to a specific configuration which has been equilibrated at 290 K for 170 ns. Then 15 uncorrelated (separated by at least 10 ns) snapshots have been selected from the resulting trajectories as starting points for production runs, after having instantaneously quenched the system from 290 to 205 K. Nucleation simulations were terminated 10 ns after a significant drop of the potential energy (>0.53 kcal/mol per water) was registered or if the simulation time exceeded 500 ns. In total, we report results from 6000 nucleation and 400 equilibration simulations.

The induction time t_n of a nucleation event has been detected by monitoring the drop in the potential energy E_{pot} of the system associated with the formation of a critical ice nucleus, as shown in Figure 2. We have calculated t_n by fitting the potential energy to

$$E_{\text{pot}}(t) = a + \frac{b}{1 + \exp[c(t - t_n)]} \quad (3)$$

where t_n , a , b , and c are fitting parameters. Due to the smoothness of the potential energy surface characterizing the mW model, crystal growth at the supercooling considered here ($\sim 70 \text{ K}$) is extremely fast, resulting in a very sharp potential energy drop that takes place within, at most, 1 ns for all values of E_{ads} and a_{fcc} considered. Thus, the resulting value of t_n does not depend on the specific shape of the fitting function. We thereby estimate the error associated with the calculation of t_n as ± 1 ns. We also verified that no substantial discrepancy with respect to t_n can be observed by using other order parameters like, e.g., the number N_{cls} of mW molecules in the biggest ice-like cluster,⁶⁹ as reported in Figure 2.

From the t_n data set, a survival probability $P_{\text{liq}}(t)$ with respect to the metastable liquid can be built, which was then fit by a stretched/compressed exponential function:

$$P_{\text{liq}}(t) = \exp[-(J \cdot t)^\gamma] \quad (4)$$

where J is the nucleation rate and γ is a parameter accounting for possible non-exponential kinetics. In fact, having quenched each

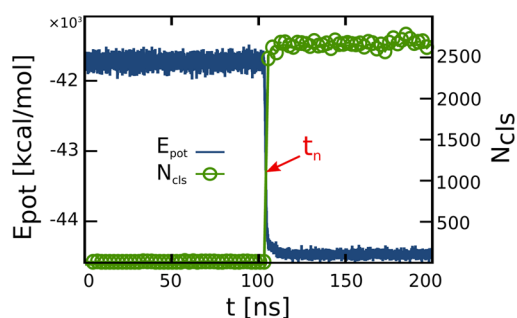


Figure 2. An illustration of how the nucleation induction time t_n is established by monitoring the change in the potential energy E_{pot} in blue. The green data show the number of water molecules within the biggest ice-like cluster N_{cls} and that the jump in N_{cls} coincides with nucleation. The data refer to the (111) surface for $E_{\text{ads}} = 1.04$ kcal/mol and $a_{\text{fcc}} = 4.16 \text{ \AA}$.

starting configuration instantaneously from 290 to 205 K, we have to take into account that the relaxation of the system, when nucleation is comparably fast, could lead to a time-dependent nucleation rate characterized by a non-exponential behavior.⁷⁰ Examples of $P_{\text{liq}}(t)$ for two very different nucleation events can be found in the Supporting Information (SI, Figure S2).

It is difficult to quantify the error in the nucleation rates from the fitting previously described. Instead, we have employed the Jackknife resampling technique⁷¹ to quantify the error associated with the finite number of simulations, and thus of induction times t_n . Jackknife resampling is particularly suitable with respect to, e.g., the conventional bootstrap approach when dealing with small sets of data. Results are reported in Figure 3. The number of simulations we have chosen

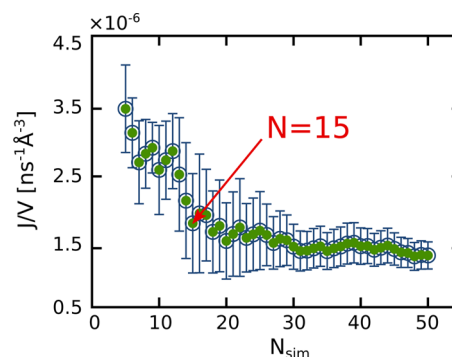


Figure 3. Illustration of the sensitivity of the nucleation rate to the number of simulations performed. Specifically the bias-corrected nucleation rate constant J/V and corresponding error bars as a function of the number of simulations N_{sim} , computed according to the Jackknife technique, are plotted. The data refer to the (111) surface ($E_{\text{ads}} = 12.7$ kcal/mol, $a_{\text{fcc}} = 3.9 \text{ \AA}$).

allows for a fairly well converged value of the nucleation rate, although an error bar accounting for about 35% of the value has to be considered. We have chosen to estimate the error bars with respect to J in the worst case scenario, namely for very mild enhancement of J with respect to the homogeneous system for which very long tails in $P_{\text{liq}}(t)$ can be observed. It must be noted that the finite size of our t_n data set is the major source of error affecting the numerical accuracy of our nucleation rates. In fact, while the calculation of both t_n and $P_{\text{liq}}(t)$ is basically error-free and finite size effects introduce a small systematic error, the long time tails of $P_{\text{liq}}(t)$ can seriously suffer from a small t_n data set because of the stochastic nature of the nucleation events.

Finite size effects must be thoroughly addressed when dealing with nucleation events. At first, we have calculated the homogeneous nucleation rate J as a function of volume for different models containing 1000, 4000, and 9000 mW molecules. We have considered

bulk liquid models as well as free-standing water slabs, in order to take into account the influence of the vacuum–water interface that we have in our slab models. The results are summarized in Figure 4 and led us

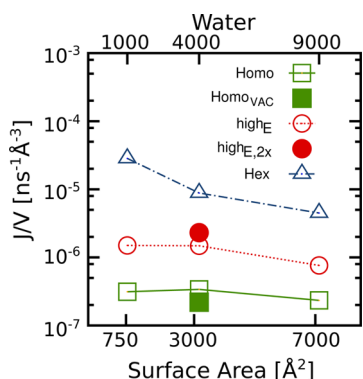


Figure 4. Nucleation rate constant J/V as a function of surface area (or number of water molecules, see x -axis, top). The legend refers to bulk homogeneous nucleation (Homo), a free-standing slab (Homo_{VAC}) with two vacuum interfaces, nucleation on top of the (111) surface (high_E , $E_{\text{ads}} = 12.7$ kcal/mol, $a_{\text{fcc}} = 3.9$ Å), same as high_E but with a water slab two times thicker ($\text{high}_{E,2x}$), and same as high_E but for $E_{\text{ads}} = 3.2$ kcal/mol where we see a hexagonal overlayer (Hex).

to choose 4000 mW molecules for our heterogeneous models. Given the fact that the heterogeneous ice nucleation rates reported in this work span 3 orders of magnitude according to the interplay between hydrophobicity and surface morphology, we can safely state that finite size effects have little impact on our results. For instance, we have verified that doubling the area of the (111) crystalline surface (and the number of water molecules as well) only introduces a discrepancy of about a factor two in the nucleation rates (normalized by surface area) for $E_{\text{ads}} = 3.21$ or 12.76 kcal/mol ($a_{\text{fcc}} = 3.90$ Å). This is somehow

expected because the strong supercooling, which should guarantee a relatively small critical nucleus size. Indeed, we have obtained an estimate of the critical nucleus for a specific case ((111) surface, $E_{\text{ads}} = 1.04$ kcal/mol, $a_{\text{fcc}} = 3.90$ Å) from a committer analysis⁷² based on the number N_{ds} of mW molecules in the biggest ice-like cluster. This suggests a critical nucleus size of about only 50 mW molecules (see SI, Figure S3). This number lies consistently in the range of literature estimates, e.g., 10 molecules at 180 K⁶⁰ and 85⁷³ to 265⁷⁴ molecules at 220 K.

3. RESULTS

3.1. No Simple Trend for Nucleation Rates. The nucleation rates on the four surfaces considered are shown as bidimensional heat maps as a function of the lattice constant and adsorption energy in Figure 5a. Regions in the 2D plots⁷⁵ for which a strong enhancement of the nucleation rates is observed are sketched in Figure 5b, and snapshots of representative trajectories for all the classified regions can be found in the SI (Figures S4–S7). Before even considering any microscopic details of the water structure or nucleation processes, several general observations about the data shown in Figure 5 can be made:

- (1) The substrates mostly do promote nucleation compared to homogeneous nucleation. On some surfaces enhancements of up to 2 orders of magnitude are seen for certain values of a_{fcc} and E_{ads} . The measured induction times for these events correspond to the transient times rather than the actual nucleation times, as discussed, e.g., by Aga et al.⁷⁶ and Peng et al.⁷⁷ Therefore, nucleation rates at the high end of the values reported should be seen as a lower bound rather than the actual rate.
- (2) Both a_{fcc} and E_{ads} do not influence nucleation on top of each surface in the same manner. Indeed, the interplay of

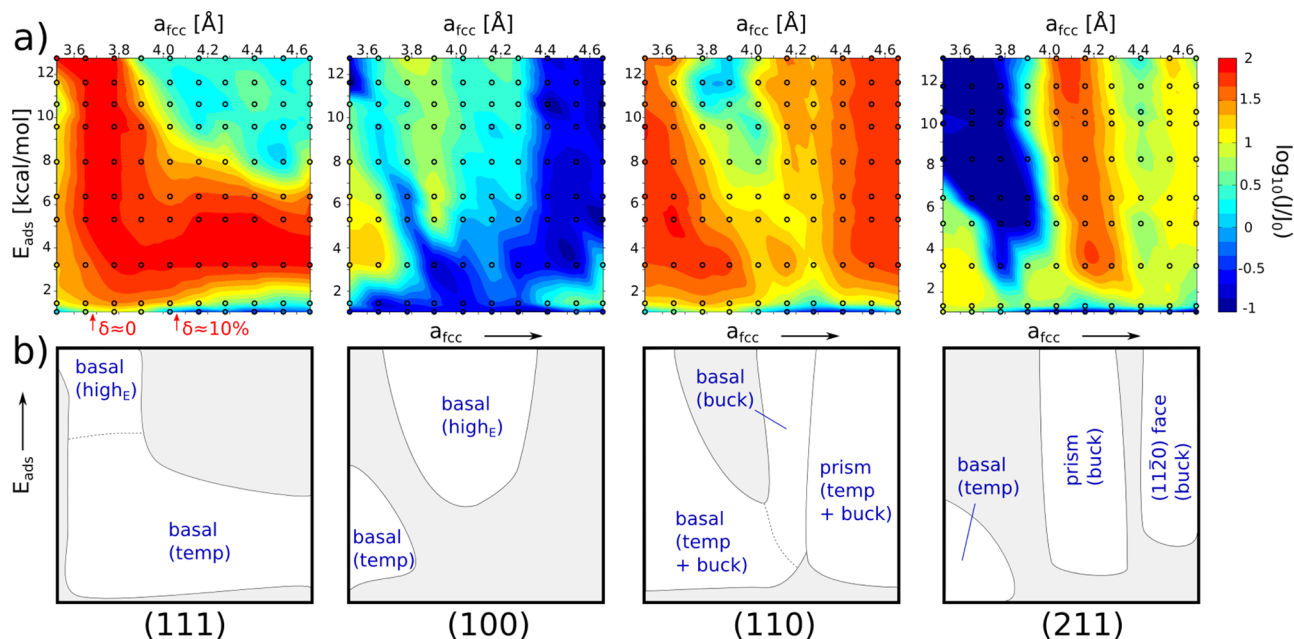


Figure 5. (a) Heat maps representing the values of ice nucleation rates on top of the four different surfaces considered, plotted as a function of the adsorption energy E_{ads} and the lattice parameter a_{fcc} . The lattice mismatch δ on (111) is indicated below the graph. The values of the nucleation rate J are reported as $\log_{10}(J/J_0)$, where J_0 refers to the homogeneous nucleation rate at the same temperature. (b) Sketches of the different regions (white areas) in the $(E_{\text{ads}}, a_{\text{fcc}})$ space in which we observe a significant enhancement of the nucleation rate. We label each region according to the face of I_h nucleating and growing on top of the surface (basal, prismatic or (11 $\bar{2}$ 0)), together with an indication of what it is that enhances the nucleation; “temp”, “buck”, and “ high_E ” refer to the in-plane template of the first overlayer, the ice-like buckling of the contact layer, and the nucleation for high adsorption energies on compact surfaces, as explained in Section 3.2.

- these two parameters is different for each surface. For instance, variation in E_{ads} for the (211) surface generally has little influence on the nucleation rate. However, on the (111) surface at certain values of a_{fcc} , variation in E_{ads} can have a very big impact on the nucleation rate.
- (3) The (111) and (110) surfaces promote ice nucleation over a much broader range than the (211) and (100) surfaces. It is worth noticing that surface symmetry alone is definitely not enough to account for such a difference. In fact, the (111) and (110) surfaces possess different symmetry (hexagonal and rectangular respectively, see Figure 1b), while the (110) and (100) surfaces, although showing completely different INA capabilities (Figure 5a), have quite comparable surface symmetry (rectangular and square, Figure 1b). Further evidence for the non-unique role of surface symmetry is given by the fact that simple trends are hard to find even within the very same surface. For instance, the interplay between a_{fcc} and E_{ads} in the case of the (110) surface results in two different regions where nucleation is significantly boosted (see Figure 5b).
 - (4) There is no optimal value for E_{ads} . In fact it is surprising how insensitive the nucleation rate is to changes in E_{ads} for some substrates such as the (110) and (211). A notable exception is the (111) surface for $a_{\text{fcc}} > 3.9 \text{ \AA}$. Our results here are consistent with the recent work of Cox et al.,^{36,37} where an optimal value of E_{ads} around 3 to 6 kcal/mol is found for a fcc(111) and a graphene nanoparticle. The broader range of a_{fcc} and the results for other substrates however reveal that this trend does not hold for the different morphologies.
 - (5) A common feature on all substrates is that the nucleation rate is inhibited for the lowest value of E_{ads} . For this adsorption energy the molecules face a hard wall which in turn could even hinder nucleation compared to the homogeneous case.^{33,78–80} By analyzing the spatial distribution of the precritical nuclei (see SI, Figure S8) we find that the latter tend not to form in the neighborhood of the water–crystal interface in the case of very low adsorption energies. Thus, this effect can be rationalized as a smaller volume available for the nuclei to appear. This volume can be estimated by the area affected by significant density perturbations due to the presence of the surface (see SI, Figure S9). This kind of inhibition is unlikely to be visible in simulations or experiments where the ratio of water volume to contact area is much higher than in our case.
 - (6) The lattice mismatch δ cannot be regarded as a requirement for an INA. This issue specifically concerns the (111) substrate, because of its compatibility with the basal face of hexagonal ice I_{h} . We calculated δ according to eq 1, the lattice constant of ice $a_{\text{i}} \approx 4.51 \text{ \AA}$ ¹⁹ and $a_{\text{s}} = \sqrt{3/2} \cdot a_{\text{fcc}}$. Therefore, a value of $a_{\text{fcc}} = 3.68 \text{ \AA}$ corresponds to a zero mismatch ($\delta = 0$) which is indicated in Figure 5a. If $\delta \approx 0$ is the main requirement for enhanced ice nucleation, we would expect a distinct peak around the corresponding value of a_{fcc} . The results for nucleation rates however clearly show that this is not the case. Certainly, a small value of δ does promote nucleation for a wider range of E_{ads} , but for adsorption energies between 2 and 6 kcal/mol, enhanced nucleation is observed for mismatches even beyond +10%. We note

that for $\delta < 0$ the drop of nucleation rates seems to start sooner than for $\delta > 0$, although the corresponding lattice constants lie outside of our considered range. This is consistent with all-atom simulations which show that a mismatch δ slightly larger than 0 is more favorable.³⁹ Furthermore, Mithen and Sear⁸¹ computed nucleation rates of a Lennard-Jones liquid in contact with a substrate and found the maximum close to but larger than $\delta = 0$. Overall, our results suggest that a small lattice mismatch is helpful to nucleation, but cannot be regarded as the most important requirement for an INA. For the other surfaces, the definition of disregistry δ is not as straightforward, because the substrates do not provide a clear template. In fact a strict definition of what can be regarded as similar or not similar is not part of the lattice mismatch theory. We have therefore restricted our discussion of the lattice mismatch to the (111) substrate.

3.2. Microscopic Factors for Nucleation. It is unexpected that a simplistic model like the one used here can foster such diverse behavior. However, when we examine the water structures and nucleation processes in detail, general trends do emerge. We now discuss the key features important to nucleation.

3.2.1. In-Plane Template of the First Overlayer. The in-plane structure of the first water overlayer plays an important role in nucleation, because it can act as a template to higher layers. This is particularly evident on the (111) surface, which possesses a hexagonal symmetry compatible with the in-plane symmetry of the basal face of ice. Where nucleation is significantly enhanced, we find that a hexagonal overlayer (HOL) of water molecules forms on top of the surface (Figure 6, “temp”), rapidly inducing nucleation. The promotion effect persists even when a significant number of defects, such as four-, five-, or seven-membered rings appear within the HOL as well as in the case of larger lattice mismatches $\delta > 0$ where the HOL is severely stretched. This indicates that the template does not have to be perfect to promote nucleation. The HOL rules the majority of nucleation processes on top of the (111) surface, where only the basal face has been observed to nucleate and grow (see Figure 5b). However, contrary to the idealized bilayer structure of the basal face the overlayers observed here are mostly flat. Reduced buckling in the contact layer has been suggested in a number of studies on metals.^{82,83} The flat hexagonal structures identified here which precede nucleation indicate that a good template needs: (i) the right symmetry and (ii) the right intermolecular distances in the plane, but not necessarily the correct water molecule heights.

We have labeled nucleation events induced by this contact layer as “temp” rather than “hex” to stress that it is not exclusively the bilayer template of the basal face, typically associated with the term HOL, but rather any possible overlayer compatible with a face of ice. An example of a different overlayer is found on the (110) surface (see SI, Figure S7) compatible with the prismatic face of ice.

3.2.2. Buckling of the First Overlayer. Our results concerning the (110) and (211) surfaces suggest that different heights of atoms in the contact layer, termed buckling, are an important factor to enhanced nucleation. The difference between a flat and a buckled overlayer can be appreciated in the water density profile along the direction normal to the surface as well as in the side views of selected trajectories, depicted in Figure 6. In the case of the “temp” mechanism, the

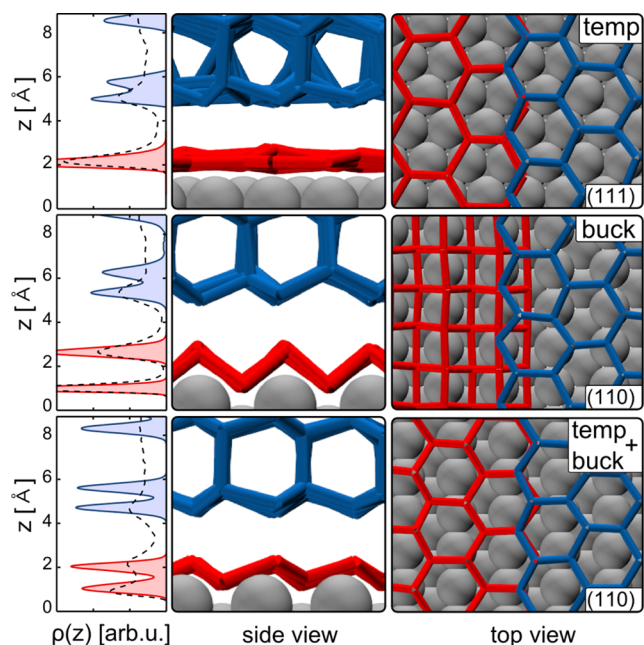


Figure 6. Analysis of certain factors important to nucleation. Each row represents data obtained from a representative trajectory for events classified as “temp”, “buck”, and both combined (“temp + buck”) mechanisms (see Section 3.2). The first column depicts the density of water molecules above the surface after freezing (filled curves) and during equilibration before freezing (dashed black line). The second column shows side views and the third column snapshots viewed from above. In all cases the contact layer is colored red, while higher layers are colored blue. For ease of visualization in the top view only part of the second layer is shown.

density profile shows a single peak only, representing the flat hexagonal contact layer. In contrast, on the (110) substrate at large lattice constants (Figure 6, “buck”), the first water

overlayer is not ice-like but exhibits a pronounced buckling of the contact layer. The fact that we find this combination of a symmetrically unfavorable (and therefore non-templating) but buckled contact layer for many of the enhanced nucleation trajectories leads us to conclude that the buckling in this case is the microscopic cause for the nucleation enhancement (labeled as “buck”).

As with the (110), the (211) geometry also leads to a significant enhancement of nucleation rates in specific regions. In addition, and quite surprisingly on this surface, nucleation and growth of three different faces of ice are observed. The three regimes roughly correspond to different values of a_{fcc} (Figure 7a). The (211) substrate has a rectangular in-plane symmetry, but it features (111) microfacets (see Figure 1a). For small values of a_{fcc} (Figure 7a), the spacing between the steps allows for rows of hexagons to form on top of these terraces. This template has a symmetry consistent with the basal face of I_h which in fact exclusively nucleates in this first regime. As an aside we note that the growth direction of the basal face is not exactly parallel to the surface normal of the (111) terraces, leading to the small angle mismatch shown in Figure 7a. As we move on to larger lattice constants, the spacing between the steps becomes too large to accommodate a hexagonal overlayer. Rather a rectangular overlayer appears on top of the surface, wiping out the templating effect of the hexagons. These overlayers are buckled in a manner that follows the corrugation of the surface. This results in the nucleation and growth of the prismatic and $(11\bar{2}0)$ faces for a_{fcc} values of 4.16 and 4.66 Å, respectively (see Figure 7a). The contact layers, despite being significantly buckled, do not show a favorable in-plane template (pictures of the overlayers can be found in the SI, Figure S5).

Thus, in the specific case of the (211) substrate, a_{fcc} is a much more sensitive parameter for the nucleation rate than E_{ads} which only leads to changes for vanishing interaction. This

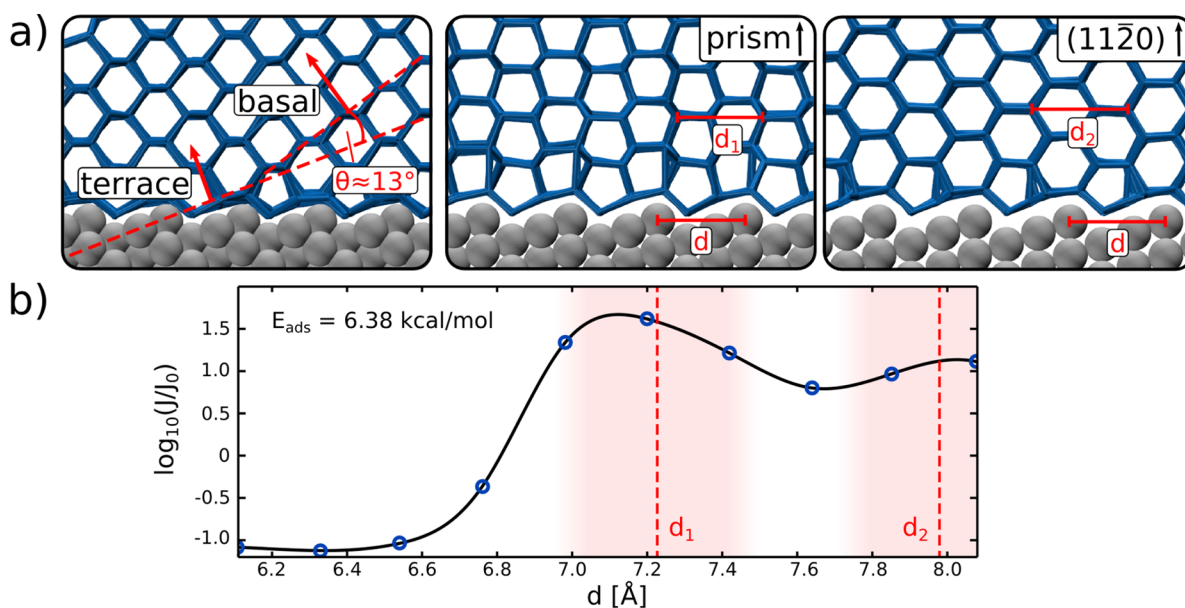


Figure 7. (a) Representative snapshots of the three different faces (basal, prismatic and $(11\bar{2}0)$ face) of hexagonal ice growing on top of the (211) surface (side view). Surface atoms are depicted as balls (gray), while the bonding network of water molecules is represented by sticks (blue). The θ angle in the top left panel illustrates that the basal face and the normal of the (111) terrace deviate. (b) Nucleation rates (circles) and spline interpolation (line) on the (211) surface as a function of the step distance d . The red lines indicate the measured characteristic distances d_1 and d_2 as well as their standard deviation (red shaded area). The meaning of d , d_1 , and d_2 is illustrated in the top panels.

suggests that nucleation enhancement due to the buckling of the overlayer is mainly regulated by geometrical motivations. Indeed, we find that the buckling of the contact layer in these cases coincides with a characteristic periodic length of one of the ice faces. To support this interpretation, in Figure 7b the nucleation rates for $E_{\text{ads}} = 6.38$ kcal/mol are displayed as a function of the step distance d . The characteristic lengths for prism and (11 $\bar{2}$ 0) face (d_1 and d_2 , respectively) were obtained from measuring and averaging the corresponding distances in representative trajectories where we see freezing of that particular ice face. The values correspond well with the step periodicity d at which nucleation is enhanced the most through formation of the respective face. A similar conclusion was drawn by Zhang et al.²⁹ for trenches promoting nucleation the most when they resemble a characteristic spacing. These effects seem to fade when the roughness is on a larger than atomic scale⁸⁴ or if the surface is amorphous.³²

The results shown in Figure 7b are reminiscent of the predictions of Turnbull and Vonnegut⁴⁷ regarding a small lattice mismatch. Indeed, if one neglects the fact that the atomic arrangements of the substrate and respective ice face at the interface are dissimilar, the buckling can be interpreted as a lattice mismatch. However, this concept is unlikely to be helpful in general as it does not clearly distinguish the two ingredients that form the buckling: (i) the different heights of atoms that are adsorbed onto the surface and; (ii) the periodicity that describes the variation of atomic heights. Contrary to the lattice mismatch, a compatible in-plane template is not required for the buckling.

We also observed nucleation events in which the overlayer possessed both atomic scale buckling and favorable in-plane template. In two specific E_{ads} and a_{fcc} intervals a buckled overlayer displaying an in-plane template consistent with the basal or prismatic face (labeled as “temp + buck”) forms on the (110) surface. The third row in Figure 6 depicts the water over layers and the corresponding density profiles in the case of basal face growth. Here, the structured water during equilibration exhibits an appearance that is already close to the double-peak of frozen (basal face) ice. The resulting overlayer consists of hexagonal arrangements, comparable to the basal face of ice not only as an in-plane template but also in the buckling. The importance of ice-like structuring along the z direction has been observed and discussed in the case of AgI.²⁸ Notably an HOL is not enough in this case, suggesting that ice-like buckling could be more effective than in-plane templating.

On the other hand, when neither the in-plane template nor the favorable buckling are present, no sizable enhancement of the nucleation rate has been observed. This is what happens for the majority of the ($E_{\text{ads}}, a_{\text{fcc}}$) points on the (100) surface (see Figure 5), which has a square symmetry and being perfectly flat does not cause the contact layer to buckle.

3.2.3. High Adsorption-Energy Nucleation on Compact Surfaces. We have also observed the promotion of nucleation in two regions where neither the ice-like in-plane template or buckling of the contact layer was present. The two regions can be found for the (111) and (100) surfaces (see Figure 5) and have been labeled high_E to emphasize that they occur only for the higher adsorption energies. It is also apparent that we find this kind of enhancement on the two compact surfaces rather than the more open ones, which suggests that it is the combination of strong interaction and surface denseness that facilitates the nucleation. The overlayers in these cases were very dense (a disordered overlayer for (111) and perfect

squares for (100), see the SI Figures S4 and S6). It is clear that these structures should be anything but advantageous for nucleation. The analysis of the distribution of precritical nuclei for a representative point (see SI, Figure S8) reveals that nucleation happened on top of the first 2–3 water layers. It is therefore clearly a heterogeneous event which the increased rates already suggested. While the actual reason for this kind of nucleation enhancement is not immediately obvious and potentially interesting, it must be noted that for values of E_{ads} in the upper third of the considered range water will probably dissociate on top of the surface rather than being adsorbed. Thus, we have not made further investigations concerning this specific enhancement. However, we suggest two possible effects that could be the driving force behind it. First, a layering mechanism similar to the one discussed by Cox et al.³⁶ could influence higher layers when the coverage of the underlying layers is saturated. This is also supported by the values of layering we have calculated, as discussed later (Section 3.3). A second reason for the facilitation could also be dynamical effects, which have been shown to significantly influence molecules and atoms near the interface.⁸⁵ The strong adsorption causes the first 1–2 layers to be nearly immobile, effectively extending the surface height and possibly shifting the dynamical effects to layers above ~ 10 Å. Lastly, we note that the effects of high_E nucleation could be shifted toward more realistic interactions for all-atom models of water, since in our tests with the TIP4P/2005 model we observed a slightly more pronounced structuring and layering (see SI, Figure S10).

3.3. Further Insight and Future Perspective. Having examined heterogeneous ice nucleation on the four crystalline substrates and identified some of the key factors responsible for the enhanced nucleation observed, we now discuss a number of open issues and ways this work could be taken forward in the future.

3.3.1. Layering. Lupi et al.^{31,32} found that the layering L of water at graphitic interfaces correlates with their freezing efficiency. For high adsorption energies Cox et al.³⁶ also found a correlation between the nucleation and the layering, but only if the layering associated with the contact layer was excluded (L^*). These two forms of layering are defined as follows:

$$L = \int_0^{z_{\text{bulk}}} \left| \frac{\rho(z)}{\rho_0} - 1 \right|^2 dz \quad (5)$$

$$L^* = \int_{z_0}^{z_{\text{bulk}}} \left| \frac{\rho(z)}{\rho_0} - 1 \right|^2 dz \quad (6)$$

where ρ_0 is the density of bulk water, z_{bulk} is the height above the surface at which the water density ρ converges to the bulk value, and z_0 is a height so that the layering contributions of the contact layer are excluded. In all cases $z_{\text{bulk}} = 18$ Å was used. The results are shown in Figure 8.

Generally, a comparison between the layering plots and the nucleation rates in Figure 5 shows that L and L^* do not correlate very well with the nucleation ability of the surface. We find that both L and L^* monotonically increase with E_{ads} . However, there seems to be a non-trivial dependency on a_{fcc} where for 3 of the 4 surfaces the layering first increases toward medium values of the lattice constant and then decreases again. This trend reflects a change of the adsorption structure of the water molecules, which was also partially the cause of the different mechanisms influencing nucleation rates. However,

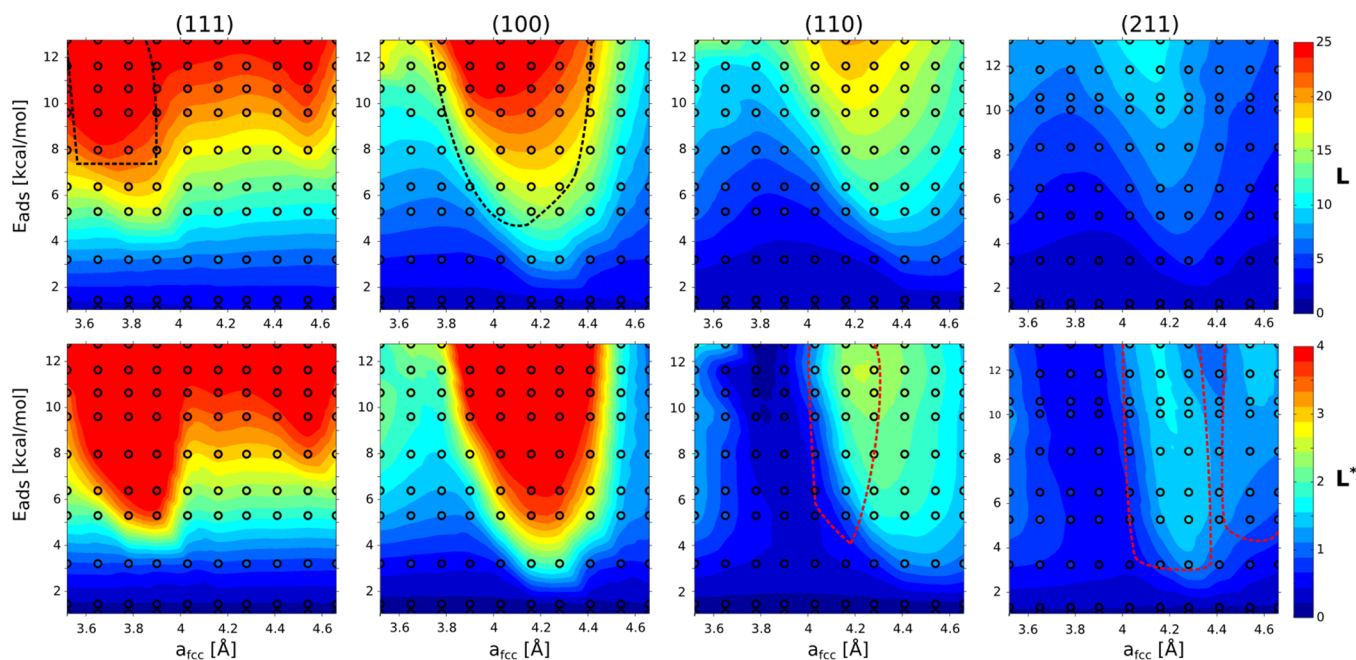


Figure 8. Heat maps representing the total layering L (top) and the layering excluding the contact layer L^* (bottom) calculated from the equilibration runs. The dashed lines indicate the regions where nucleation was enhanced through high $_E$ nucleation (black) and buckling (red). Note that the color range for L and L^* is different.

the trends of the nucleation maps are not reproduced. For instance, no region that has been classified as “temp” can be distinguished from its surrounding in the layering plots. If one assumes an optimal value or threshold for L or L^* , the corresponding iso-surfaces in the plot would not reproduce any plot of the nucleation rates. While this conclusion has already started to emerge from the work of Cox et al.,³⁶ we can now base the argumentation on a much larger parameter space and additional surfaces.

Interestingly, we find some exceptions. Specifically the areas classified as high $_E$ nucleation seem to be similar to areas of strong layering. This could also explain why we do not see this mechanism on the (110) and (211) surfaces, because the layering is still too weak even for the highest adsorption energies. Also the L^* plot for the (211) substrate seems to indicate the regions that have been classified as “buck”. However, no quantitative agreement is found, as for instance $L^* \approx 2$ on the (110) surface shapes a region where nucleation rates differ by an order of magnitude.

Overall, we find that the layering does not generally correlate with the nucleation ability which is likely due to the fact that this quantity averages over lateral structure effects such as the in-plane symmetry and template. The exceptions are such cases where the potential energy surface is smooth, as for instance high $_E$ events where nucleation happens further away from the surface or nucleation on graphene-like surfaces.^{31,36}

3.3.2. Notes on the Water Model. The fast dynamics associated with the coarse-grained mW model has made the current systematic study possible. However, it is important to consider, at the very least, how the absence of explicit hydrogens affects the results of this study. To this end, we have performed test calculations with the all-atom TIP4P/2005 model⁸⁶ which provides a reasonable description of water.⁸⁷

First, we compared the water densities for one (a_{fcc}, E_{ads}) point on each surface (see SI, Figure S10). The densities

obtained are very similar for both water models, and we conclude that the structuring they show is nearly equivalent.

Second, a set of nucleation simulations with the all-atom model was carried out on the (111) surface. Here, the almost instantaneous formation of a hexagonal overlayer was the driving force behind the nucleation enhancement for mW. With TIP4P/2005 we did not observe the complete formation of such an overlayer within 100 ns. However, an analysis of the hexagonal cluster distribution (see SI, Figure S11) shows that the largest patches of hexagons can be found for $E_{ads} \approx 3.2$ kcal/mol. This is precisely the value for which we observe the fastest formation in the case of mW as well.⁸⁸ This trend confirms that while - especially heterogeneous - nucleation processes modeled by mW water are for certain non-physically fast, they can still capture part of the underlying physics.

3.3.3. Higher Temperatures. It is interesting to understand how the trends observed in this study could depend on temperature, especially because our simulations were performed in the deeply supercooled regime. It is currently beyond our reach to carry out such an extensive set of simulations at a significantly higher temperature with the brute-force approach. However, to estimate the effect of the strong supercooling we performed further calculations at 210 and 215 K for 3 adsorption energies on the (110) surface (the results can be found in the SI, Figure S12). We find that the nucleation rates in regions where no specific mechanism has been attributed heavily decline, but otherwise no significant changes can be observed. That includes the trends of the nucleation rate as well as the adsorption structures, which are the basis for the mechanisms we propose. This indicates that our conclusions are also valid for higher temperatures.

3.3.4. Future Perspective and Experimental Verification. Before concluding we discuss some aspects that should be addressed in future studies as well as making some suggestions about how the insight presented here could be tested experimentally.

A first step will be to use all-atom models of water^{87,89} such as the TIP4P/2005 discussed above or its cousin TIP4P/Ice⁹⁰ specifically designed for the study of ice. Recently all-atom simulations of homogeneous ice nucleation have been performed⁹¹ with the help of the forward-flux sampling technique.^{92,93} The latter seems like a promising approach for nucleation simulations,^{35,73,78,91,94–96} although there are of course many other free energy and enhanced sampling techniques^{72,97–104} that could be used. Improvement in the water–surface interaction potential is of equal importance if one wishes to investigate heterogeneous ice nucleation. For instance, an extension of the present study to realistic clean metal surfaces needs to account for the orientational dependence of the water molecules on the surface and polarization effects. Fitting water–surface interaction potentials to DFT or higher-level electronic structure theories is one way to take such effects into account, and work in our group in this direction is ongoing.^{65,105–107} In the attempt to take another step toward the modeling of realistic surfaces, the effect of surface vibrations, structural relaxation, and surface reconstruction, together with the influence of surface defects, must be taken into account and will be the focus of future computational efforts. Furthermore, it has been shown that dissociation of water molecules occurs at reactive metal surfaces so that the overlayers can be comprised of water-hydroxyl mixtures.^{108–111} Taking this issue into account will require a suitable and accurate dissociable model of water. Lastly, it will be important that nucleation studies approach experiments more closely. Especially the supercooling in computational studies is a major concern since it is too strong to directly allow for comparison with, e.g., atmospheric or laboratory measurements.

Our results could be most directly probed by measurements that can reliably characterize surface structures with molecular level of resolution. This would require ultrahigh vacuum prepared levels of cleanliness. A most promising candidate for an experimental study would be gold surfaces because of their resistance to oxidation and gold's fcc crystal structure. With $a_{\text{fcc}} \approx 4.08 \text{ \AA}$ ¹¹² and $E_{\text{ads}} \approx 3\text{--}7 \text{ kcal/mol}$,⁶⁵ our simulations indicate that the nucleation rates on the (111) and (100) gold substrates should differ by 2–3 orders of magnitude. This has been estimated from the data in Figure 5 in the region of the Au lattice constant and E_{ads} .¹¹³ This would also allow the control of nucleation on gold (and other) nanoparticles that expose different facets. By adding molecules that are inactive for ice nucleation but selectively bind to the promoting facets of the particle, the nucleation rate could be controlled. Indications of freezing in a well-defined surface-science-style study could be obtained with, e.g., ambient pressure X-ray photoelectron spectroscopy^{114,115} or surface X-ray diffraction.¹¹⁶ Another class of interesting materials are halogenated graphene^{117,118} and graphene.¹¹⁹ The functionalization of graphene with different atoms such as H, F, Cl, Br or I should alter the underlying geometry of the 2D material only slightly,^{120,121} but the water–surface interaction could greatly vary.¹²² This could be exploited to verify our predictions for different interaction strengths by examining ice nucleation on these compounds. This idea can even be extended to other quasi-2D honeycomb materials such as silicene,¹²³ germanene,¹²⁴ and stanene¹²⁵ that have different lattice constants^{122,126} if grown on appropriate supports and if they remain stable in an aqueous environment. In such a manner the interplay between morphology and hydrophobicity could be examined experimentally, possibly yielding a similar nucleation map to Figure 5a. Moreover, self-

assembled monolayers^{127–129} provide the possibility to create specific morphologies. For instance different headgroups for aliphatic chains can alter the hydrophobicity of the resulting surface, while functional groups in the chain can change the spacing between them. Additionally, different chain lengths could be used to design a buckled surface. In combination with non-hydrogen-bonding headgroups, this could enable the design of interfaces useful for testing the buckling mechanism. Finally, we note that the exciting capabilities of femtosecond X-ray scattering^{130,131} techniques, that have recently been used to explore homogeneous ice formation in water droplets, could possibly be extended to heterogeneous systems.

4. CONCLUSIONS

In summary, we have examined the interplay between surface morphology and hydrophobicity on the ability of a generic crystalline surface to promote ice nucleation. We have calculated the nucleation rates of a coarse-grained model of water on top of four different crystalline surfaces of an ideal fcc crystal by means of brute-force MD simulations, sweeping a comprehensive range of adsorption energies and lattice parameters.

Strikingly different nucleation scenarios have emerged on the various crystalline surfaces considered. Even for a specific surface the balance between lattice constant and hydrophobicity fosters non-trivial trends. Most surprisingly the nucleation and growth of up to three different faces of hexagonal ice on top of the same surface could be induced by altering the lattice parameter alone.

We have demonstrated that on the (111) surface a small lattice mismatch with respect to ice is certainly not a requirement for promoting ice nucleation. This implies that in the search for understanding of the nucleation performance of known materials or the design of new ones, one should not exclusively focus on the lattice mismatch issue. Nonetheless, our results show that it is important which surface is present, as nucleation rates can vary from inhibition to promotion for different faces of the same material. This means that experiments have to carefully characterize the atomic structure of INAs, because the sheer morphological difference in samples could account for varying nucleation rates. Additionally, this provides exciting possibilities to change the ice nucleation behavior of materials through, e.g., growth-habit control¹³² to strengthen the inhibition effect or to turn nucleating nanoparticles into inhibitors and vice versa.

In most cases nucleation is promoted in a wide range of E_{ads} without changing the molecular mechanism. Therefore, optimal interaction strengths are rare exceptions and only found for some specific a_{fcc} ranges.

Finally, we have pinpointed three different scenarios that facilitate the nucleation process:

- (1) The ability of the surface to create a first water overlayer that provides an in-plane template consistent with one of the faces of ice. Such an overlayer is typically, but not exclusively, found on top of a surface that already displays a compatible symmetry.
- (2) The ability of the surface to structure the first two water overlayers in such a way that they resemble either the density profile perpendicular to the surface or a characteristic buckling distance in the surface plane of one of the faces of ice. This typically requires a certain roughness at the atomic scale.

- (3) Even in the case of a first overlayer lacking both an in-plane template and structuring, nucleation can be promoted within the higher water layers. This kind of enhancement requires a compact surface with high adsorption energy.

Whether or not one of these scenarios could take place on top of a given surface depends in a non-trivial manner on both the morphology and hydrophobicity of the surface. Such a large body of findings will hopefully encourage and guide future work addressing heterogeneous ice nucleation on top of realistic surfaces, in the hope of furthering our understanding of what makes a material a good INA.

■ ASSOCIATED CONTENT

■ Supporting Information

The Supporting Information is available free of charge on the ACS Publications website at DOI: 10.1021/jacs.5b08748.

Distribution of the $\bar{q}_3(i)$ order parameter used for calculating N_{cls} , examples for dissimilar stretched exponential fits, critical nucleus size on the (111) substrate, snapshots of all classified regions, distribution of precritical nuclei, verification of the water model, notes on higher temperatures (PDF)

■ AUTHOR INFORMATION

Corresponding Author

*angelos.michaelides@ucl.ac.uk

Notes

The authors declare no competing financial interest.

■ ACKNOWLEDGMENTS

This work was supported by the European Research Council under the European Union's Seventh Framework Programme (FP/2007-2013)/ERC Grant Agreement number 616121 (HeteroIce project). A.M. is also supported by the Royal Society through a Royal Society Wolfson Research Merit Award. Dr. A. Zen and P. Pedevilla are thanked for insightful discussions. We thank Dr. Ben Slater for commenting on the original manuscript. We are grateful for computational resources provided by the London Centre for Nanotechnology and the Materials Chemistry Consortium through the EPSRC grant number EP/L000202.

■ REFERENCES

- (1) Murray, B. J.; O'Sullivan, D.; Atkinson, J. D.; Webb, M. E. *Chem. Soc. Rev.* **2012**, *41*, 6519–6554.
- (2) Bartels-Rausch, T. *Nature* **2013**, *494*, 27–29.
- (3) Mazur, P. *Science* **1970**, *168*, 939–949.
- (4) Lintunen, A.; Hölttä, T.; Kulmala, M. *Sci. Rep.* **2013**, *3*, 2031.
- (5) Hegg, D. A.; Baker, M. B. *Rep. Prog. Phys.* **2009**, *72*, 056801.
- (6) Bartels-Rausch, T.; Bergeron, V.; Cartwright, J. H. E.; Escribano, R.; Finney, J. L.; Grothe, H.; Gutiérrez, P. J.; Haapala, J.; Kuhs, W. F.; Pettersson, J. B. C.; Price, S. D.; Sainz-Díaz, C. I.; Stokes, D. J.; Strazzulla, G.; Thomson, E. S.; Trinks, H.; Uras-Aytemiz, N. *Rev. Mod. Phys.* **2012**, *84*, 885–944.
- (7) Finnegan, W. G.; Chai, S. K. *J. Atmos. Sci.* **2003**, *60*, 1723–1731.
- (8) Michaelides, A.; Morgenstern, K. *Nat. Mater.* **2007**, *6*, 597–601.
- (9) Zobrist, B.; Marcolli, C.; Peter, T.; Koop, T. *J. Phys. Chem. A* **2008**, *112*, 3965–3975.
- (10) Zimmermann, F.; Weinbruch, S.; Schütz, L.; Hofmann, H.; Ebert, M.; Kandler, K.; Worringer, A. *J. Geophys. Res.* **2008**, *113*, D23204.
- (11) Murray, B. J.; Wilson, T. W.; Dobbie, S.; Cui, Z.; Al-Jumur, S. M. R. K.; Möhler, O.; Schnaiter, M.; Wagner, R.; Benz, S.; Niemand, M.; Saathoff, H.; Ebert, V.; Wagner, S.; Kärcher, B. *Nat. Geosci.* **2010**, *3*, 233–237.
- (12) Ehre, D.; Lavert, E.; Lahav, M.; Lubimirsky, I. *Science* **2010**, *327*, 672–675.
- (13) Murray, B. J.; Broadley, S. L.; Wilson, T. W.; Atkinson, J. D.; Wills, R. H. *Atmos. Chem. Phys.* **2011**, *11*, 4191–4207.
- (14) Knopf, D. A.; Alpert, P. A.; Wang, B.; Aller, J. Y. *Nat. Geosci.* **2011**, *4*, 88–90.
- (15) Tobo, Y.; DeMott, P. J.; Raddatz, M.; Niedermeier, D.; Hartmann, S.; Kreidenweis, S. M.; Stratmann, F.; Wex, H. *Geophys. Res. Lett.* **2012**, *39*, L19803.
- (16) Li, K.; Xu, S.; Shi, W.; He, M.; Li, H.; Li, S.; Zhou, X.; Wang, J.; Song, Y. *Langmuir* **2012**, *28*, 10749–10754.
- (17) Fu, Q. T.; Liu, E. J.; Wilson, P.; Chen, Z. *Phys. Chem. Chem. Phys.* **2015**, *17*, 21492–21500.
- (18) Whale, T. F.; Rosillo-Lopez, M.; Murray, B. J.; Salzmann, C. G. *J. Phys. Chem. Lett.* **2015**, *6*, 3012–3016.
- (19) Pruppacher, H.; Klett, J. *Microphysics of Clouds and Precipitation*; Atmospheric and Oceanographic Sciences Library; Springer: The Netherlands, 1997.
- (20) Pratt, K. A.; DeMott, P. J.; French, J. R.; Wang, Z.; Westphal, D. L.; Heymsfield, A. J.; Twohy, C. H.; Prenni, A. J.; Prather, K. A. *Nat. Geosci.* **2009**, *2*, 398–401.
- (21) Pratt, K. A.; Heymsfield, A. J.; Twohy, C. H.; Murphy, S. M.; DeMott, P. J.; Hudson, J. G.; Subramanian, R.; Wang, Z.; Seinfeld, J. H.; Prather, K. A. *J. Atmos. Sci.* **2010**, *67*, 2451–2468.
- (22) Hoose, C.; Möhler, O. *Atmos. Chem. Phys. Discuss.* **2012**, *12*, 12531–12621.
- (23) Atkinson, J. D.; Murray, B. J.; Woodhouse, M. T.; Whale, T. F.; Baustian, K. J.; Carslaw, K. S.; Dobbie, S.; O'Sullivan, D.; Malkin, T. L. *Nature* **2013**, *498*, 355–358.
- (24) Hiranuma, N.; Möhler, O.; Yamashita, K.; Tajiri, T.; Saito, A.; Kiselev, A.; Hoffmann, N.; Hoose, C.; Jantsch, E.; Koop, T.; Murakami, M. *Nat. Geosci.* **2015**, *8*, 273–277.
- (25) Moore, E. B.; de la Llave, E.; Welke, K.; Scherlis, D. A.; Molinero, V. *Phys. Chem. Chem. Phys.* **2010**, *12*, 4124–4134.
- (26) Yan, J. Y.; Patey, G. N. *J. Phys. Chem. A* **2012**, *116*, 7057–7064.
- (27) Hudait, A.; Molinero, V. *J. Am. Chem. Soc.* **2014**, *136*, 8081–8093.
- (28) Zielke, S. A.; Bertram, A. K.; Patey, G. N. *J. Phys. Chem. B* **2015**, *119*, 9049–9055.
- (29) Zhang, X.-X.; Chen, M.; Fu, M. *J. Chem. Phys.* **2014**, *141*, 124709.
- (30) Singh, J. K.; Müller-Plathe, F. *Appl. Phys. Lett.* **2014**, *104*, 021603.
- (31) Lupi, L.; Molinero, V. *J. Phys. Chem. A* **2014**, *118*, 7330–7337.
- (32) Lupi, L.; Hudait, A.; Molinero, V. *J. Am. Chem. Soc.* **2014**, *136*, 3156–3164.
- (33) Reinhardt, A.; Doye, J. P. K. *J. Chem. Phys.* **2014**, *141*, 084501.
- (34) Fraux, G.; Doye, J. P. K. *J. Chem. Phys.* **2014**, *141*, 216101.
- (35) Cabriolu, R.; Li, T. *Phys. Rev. E* **2015**, *91*, 052402.
- (36) Cox, S. J.; Kathmann, S. M.; Slater, B.; Michaelides, A. *J. Chem. Phys.* **2015**, *142*, 184705.
- (37) Cox, S. J.; Kathmann, S. M.; Slater, B.; Michaelides, A. *J. Chem. Phys.* **2015**, *142*, 184704.
- (38) Hu, X. L.; Michaelides, A. *Surf. Sci.* **2007**, *601*, 5378–5381.
- (39) Cox, S. J.; Kathmann, S. M.; Purton, J. A.; Gillan, M. J.; Michaelides, A. *Phys. Chem. Chem. Phys.* **2012**, *14*, 7944–7949.
- (40) Pirzadeh, P.; Kusalik, P. G. *J. Am. Chem. Soc.* **2013**, *135*, 7278–7287.
- (41) Cox, S. J.; Raza, Z.; Kathmann, S. M.; Slater, B.; Michaelides, A. *Faraday Discuss.* **2014**, *167*, 389–403.
- (42) Factorovich, M. H.; Molinero, V.; Scherlis, D. A. *J. Am. Chem. Soc.* **2015**, *137*, 10618–10623.
- (43) Hribar, B.; Southall, N. T.; Vlachy, V.; Dill, K. A. *J. Am. Chem. Soc.* **2002**, *124*, 12302–12311.

- (44) Reveles, J. U.; Calaminici, P.; Beltrán, M. R.; Köster, A. M.; Khanna, S. N. *J. Am. Chem. Soc.* **2007**, *129*, 15565–15571.
- (45) Yan, J. Y.; Patey, G. N. *J. Phys. Chem. Lett.* **2011**, *2*, 2555–2559.
- (46) Nistor, R. A.; Markland, T. E.; Berne, B. J. *J. Phys. Chem. B* **2014**, *118*, 752–760.
- (47) Turnbull, D.; Vonnegut, B. *Ind. Eng. Chem.* **1952**, *44*, 1292–1298.
- (48) Vonnegut, B. *J. Appl. Phys.* **1947**, *18*, 593–595.
- (49) Zettlemoyer, A. C.; Tcheurekdjian, N.; Chessick, J. J. *Nature* **1961**, *192*, 653–653.
- (50) Kajava, A. V.; Lindow, S. E. *J. Mol. Biol.* **1993**, *232*, 709–717.
- (51) Murakami, D.; Yasuoka, K. *J. Chem. Phys.* **2012**, *137*, 054303.
- (52) Gorbunov, B.; Baklanov, A.; Kakutkina, N.; Windsor, H. L.; Toumi, R. *J. Aerosol Sci.* **2001**, *32*, 199–215.
- (53) Dymarska, M.; Murray, B. J.; Sun, L.; Eastwood, M. L.; Knopf, D. A.; Bertram, A. K. *J. Geophys. Res.* **2006**, *111*, D04204.
- (54) Kärcher, B.; Möhler, O.; DeMott, P. J.; Pechtl, S.; Yu, F. *Atmos. Chem. Phys.* **2007**, *7*, 4203–4227.
- (55) Friedman, B.; Kulkarni, G.; Beránek, J.; Zelenyuk, A.; Thornton, J. A.; Cziczo, D. J. *J. Geophys. Res.* **2011**, *116*, D17203.
- (56) Bingemer, H.; Klein, H.; Ebert, M.; Haunold, W.; Bundke, U.; Herrmann, T.; Kandler, K.; Müller-Ebert, D.; Weinbruch, S.; Judt, A.; Weber, A.; Nillius, B.; Ardon-Dryer, K.; Levin, Z.; Curtius, J. *Atmos. Chem. Phys.* **2012**, *12*, 857–867.
- (57) Cabrera-Sanfeli, P.; Darling, G. R. *J. Phys. Chem. C* **2007**, *111*, 18258–18263.
- (58) Molinero, V.; Moore, E. B. *J. Phys. Chem. B* **2009**, *113*, 4008–4016.
- (59) Moore, E. B.; Molinero, V. *J. Chem. Phys.* **2010**, *132*, 244504.
- (60) Moore, E. B.; Molinero, V. *Phys. Chem. Chem. Phys.* **2011**, *13*, 20008–20016.
- (61) Johnston, J. C.; Molinero, V. *J. Am. Chem. Soc.* **2012**, *134*, 6650–6659.
- (62) All systems were built with the python.ASE¹³³ and VMD¹³⁴ software packages.
- (63) Fajin, J. L. C.; Cordeiro, M. N. D. S.; Gomes, J. R. B. *J. Phys. Chem. A* **2014**, *118*, 5832–5840.
- (64) This result was not dependent and could not be avoided by different minimization algorithms (steepest descent, conjugate gradient, and Hessian-free truncated Newton as implemented in LAMMPS).⁶⁶
- (65) Carrasco, J.; Klimeš, J.; Michaelides, A. *J. Chem. Phys.* **2013**, *138*, 024708.
- (66) Plimpton, S. J. *Comput. Phys.* **1995**, *117*, 1–19.
- (67) Nosé, S. *J. Chem. Phys.* **1984**, *81*, 511–519.
- (68) Martyna, G. J.; Klein, M. L.; Tuckerman, M. J. *J. Chem. Phys.* **1992**, *97*, 2635–2643.
- (69) In the definition of N_{cls} we label the i -th mW molecule as ice-like according to the order parameter $\bar{q}_3(i)$ as described by Lechner and Dellago,¹³⁵ using a radial cutoff of 3.2 Å. Two ice-like molecules are considered connected up to the same cutoff as above. The distribution of the $\bar{q}_3(i)$ parameter can be found in the SI (Figure S1).
- (70) Sear, R. P. *CrystEngComm* **2014**, *16*, 6506–6522.
- (71) Tukey, J. W. *Ann. Math. Stat.* **1958**, 614–614.
- (72) Bolhuis, P. G.; Chandler, D.; Dellago, C.; Geissler, P. L. *Annu. Rev. Phys. Chem.* **2002**, *53*, 291–318.
- (73) Li, T.; Donadio, D.; Russo, G.; Galli, G. *Phys. Chem. Chem. Phys.* **2011**, *13*, 19807–19813.
- (74) Reinhardt, A.; Doye, J. P. K. *J. Chem. Phys.* **2012**, *136*, 054501.
- (75) The 10×10 mesh of obtained values for each surface was first interpolated from the non-regular to a regular grid via a 2D-spline interpolation. Then this picture was resized to an image with 20 times finer resolution with the lanczos3 algorithm as implemented in MATLAB.^{136,137}
- (76) Aga, R. S.; Morris, J. R.; Hoyt, J. J.; Mendeleev, M. *Phys. Rev. Lett.* **2006**, *96*, 245701.
- (77) Peng, L. J.; Morris, J. R.; Aga, R. S. *J. Chem. Phys.* **2010**, *133*, 084505.
- (78) Haji-Akbari, A.; DeFever, R. S.; Sarupria, S.; Debenedetti, P. G. *Phys. Chem. Chem. Phys.* **2014**, *16*, 25916–25927.
- (79) Zhang, H.; Peng, S.; Mao, L.; Zhou, X.; Liang, J.; Wan, C.; Zheng, J.; Ju, X. *Phys. Rev. E* **2014**, *89*, 062410.
- (80) Zhang, H.; Peng, S.; Long, X.; Zhou, X.; Liang, J.; Wan, C.; Zheng, J.; Ju, X. *Phys. Rev. E* **2014**, *89*, 032412.
- (81) Mithen, J. P.; Sear, R. P. *J. Chem. Phys.* **2014**, *140*, 084504.
- (82) Ogasawara, H.; Brena, B.; Nordlund, D.; Nyberg, M.; Pelmeshnikov, A.; Pettersson, L. G. M.; Nilsson, A. *Phys. Rev. Lett.* **2002**, *89*, 276102.
- (83) Michaelides, A.; Alavi, A.; King, D. A. *Phys. Rev. B: Condens. Matter Mater. Phys.* **2004**, *69*, 113404.
- (84) Campbell, J. M.; Meldrum, F. C.; Christenson, H. K. *J. Phys. Chem. C* **2015**, *119*, 1164–1169.
- (85) Haji-Akbari, A.; Debenedetti, P. G. *J. Chem. Phys.* **2014**, *141*, 024506.
- (86) Abascal, J. L. F.; Vega, C. *J. Chem. Phys.* **2005**, *123*, 234505.
- (87) Vega, C.; Abascal, J. L. F. *Phys. Chem. Chem. Phys.* **2011**, *13*, 19663–19688.
- (88) To vaporize interaction energies for different water models, the heat of vaporization is often used. The latter for both models is nearly the same,^{58,86} which means we can compare the adsorption energies directly.
- (89) Sanz, E.; Vega, C.; Espinosa, J. R.; Caballero-Bernal, R.; Abascal, J. L. F.; Valeriani, C. *J. Am. Chem. Soc.* **2013**, *135*, 15008–15017.
- (90) Abascal, J. L. F.; Sanz, E.; Fernández, R. G.; Vega, C. *J. Chem. Phys.* **2005**, *122*, 234511.
- (91) Haji-Akbari, A.; Debenedetti, P. G. *Proc. Natl. Acad. Sci. U. S. A.* **2015**, *112*, 10582–10588.
- (92) Allen, R. J.; Frenkel, D.; Wolde, P. R. *J. Chem. Phys.* **2006**, *124*, 024102.
- (93) Allen, R. J.; Valeriani, C.; Wolde, P. R. *J. Phys.: Condens. Matter* **2009**, *21*, 463102.
- (94) Li, T.; Donadio, D.; Galli, G. *Nat. Commun.* **2013**, *4*, 1887.
- (95) Jiang, H.; Pu, M.; Hou, Z. *Sci. China: Chem.* **2014**, *57*, 165–171.
- (96) Bi, Y.; Li, T. *J. Phys. Chem. B* **2014**, *118*, 13324–13332.
- (97) Torrie, G. M.; Valleau, J. P. *J. Comput. Phys.* **1977**, *23*, 187–199.
- (98) Mezei, M. *J. Comput. Phys.* **1987**, *68*, 237–248.
- (99) Laio, A.; Parrinello, M. *Proc. Natl. Acad. Sci. U. S. A.* **2002**, *99*, 12562–12566.
- (100) Laio, A.; Gervasio, F. L. *Rep. Prog. Phys.* **2008**, *71*, 126601.
- (101) Kästner, J. *Wiley Interdiscip. Rev.: Comput. Mol. Sci.* **2011**, *1*, 932–942.
- (102) Zheng, W.; Rohrdanz, M. A.; Clementi, C. *J. Phys. Chem. B* **2013**, *117*, 12769–12776.
- (103) Dittmar, H.; Kusalik, P. G. *Phys. Rev. Lett.* **2014**, *112*, 195701.
- (104) Tiwary, P.; Parrinello, M. *J. Phys. Chem. B* **2015**, *119*, 736–742.
- (105) Ma, J.; Michaelides, A.; Alfè, D.; Schimka, L.; Kresse, G.; Wang, E. *Phys. Rev. B: Condens. Matter Mater. Phys.* **2011**, *84*, 033402.
- (106) Al-Hamdani, Y. S.; Alfè, D.; Lilienfeld, O. A. v.; Michaelides, A. *J. Chem. Phys.* **2014**, *141*, 18C530.
- (107) Al-Hamdani, Y. S.; Ma, M.; Alfè, D.; Lilienfeld, O. A. v.; Michaelides, A. *J. Chem. Phys.* **2015**, *142*, 181101.
- (108) Michaelides, A.; Hu, P. *J. Am. Chem. Soc.* **2001**, *123*, 4235–4242.
- (109) Feibelman, P. J. *Science* **2002**, *295*, 99–102.
- (110) Forster, M.; Raval, R.; Hodgson, A.; Carrasco, J.; Michaelides, A. *Phys. Rev. Lett.* **2011**, *106*, 046103.
- (111) Carrasco, J.; Hodgson, A.; Michaelides, A. *Nat. Mater.* **2012**, *11*, 667–674.
- (112) *WolframAlpha*; Wolfram Alpha LLC: Champaign, IL, <http://reference.wolfram.com/language/ref/ElementData.html> (access date July 19, 2015).
- (113) The actual difference in nucleation rates for Au(111) and Au(100) could be even larger, since the highest nucleation rates computed in our study are only lower bounds. Therefore a significant difference between these two substrates should also be detectable if one measures freezing temperatures.

- (114) Bluhm, H.; Ogletree, D. F.; Fadley, C. S.; Hussain, Z.; Salmeron, M. *J. Phys.: Condens. Matter* **2002**, *14*, L227.
- (115) Ketteler, G.; Yamamoto, S.; Bluhm, H.; Andersson, K.; Starr, D. E.; Ogletree, D. F.; Ogasawara, H.; Nilsson, A.; Salmeron, M. *J. Phys. Chem. C* **2007**, *111*, 8278–8282.
- (116) Gustafson, J.; Shipilin, M.; Zhang, C.; Stierle, A.; Hejral, U.; Ruett, U.; Gutowski, O.; Carlsson, P.-A.; Skoglundh, M.; Lundgren, E. *Science* **2014**, *343*, 758–761.
- (117) Lu, D.; Yang, Y.-R.; Xiao, Y.; Zhang, X.-Y. *Chin. Phys. B* **2011**, *20*, 118101.
- (118) Georgakilas, V.; Otyepka, M.; Bourlinos, A. B.; Chandra, V.; Kim, N.; Kemp, K. C.; Hobza, P.; Zboril, R.; Kim, K. S. *Chem. Rev.* **2012**, *112*, 6156–6214.
- (119) Elias, D. C.; Nair, R. R.; Mohiuddin, T. M. G.; Morozov, S. V.; Blake, P.; Halsall, M. P.; Ferrari, A. C.; Boukhvalov, D. W.; Katsnelson, M. I.; Geim, A. K.; Novoselov, K. S. *Science* **2009**, *323*, 610–613.
- (120) Medeiros, P. V. C.; Mascarenhas, A. J. S.; Mota, F. d. B.; Castilho, C. M. C. d. *Nanotechnology* **2010**, *21*, 485701.
- (121) Gao, N.; Zheng, W. T.; Jiang, Q. *Phys. Chem. Chem. Phys.* **2011**, *14*, 257–261.
- (122) Garcia, J. C.; de Lima, D. B.; Assali, L. V. C.; Justo, J. F. *J. Phys. Chem. C* **2011**, *115*, 13242–13246.
- (123) Vogt, P.; de Padova, P.; Quaresima, C.; Avila, J.; Frantzeskakis, E.; Asensio, M. C.; Resta, A.; Ealet, B.; le Lay, G. *Phys. Rev. Lett.* **2012**, *108*, 155501.
- (124) Dávila, M. E.; Xian, L.; Cahangirov, S.; Rubio, A.; Lay, G. L. *New J. Phys.* **2014**, *16*, 095002.
- (125) Zhu, F. F.; Chen, W. J.; Xu, Y.; Gao, C. L.; Guan, D. D.; Liu, C. H.; Qian, D.; Zhang, S. C.; Jia, J. F. *Nat. Mater.* **2015**, *14*, 1020–1025.
- (126) Wei, W.; Dai, Y.; Huang, B.; Jacob, T. *Phys. Chem. Chem. Phys.* **2013**, *15*, 8789–8794.
- (127) Seeley, L. H.; Seidler, G. T. *Phys. Rev. Lett.* **2001**, *87*, 055702.
- (128) Arnold, R.; Azzam, W.; Terfort, A.; Wöll, C. *Langmuir* **2002**, *18*, 3980–3992.
- (129) Ochshorn, E.; Cantrell, W. *J. Chem. Phys.* **2006**, *124*, 054714.
- (130) Sellberg, J. A.; Huang, C.; McQueen, T. A.; Loh, N. D.; Laksmono, H.; Schlesinger, D.; Sierra, R. G.; Nordlund, D.; Hampton, C. Y.; Starodub, D.; DePonte, D. P.; Beyre, M.; Chen, C.; Martin, A. V.; Barty, A.; Wikfeldt, K. T.; Weiss, T. M.; Caronna, C.; Feldkamp, J.; Skinner, L. B.; Seibert, M. M.; Messerschmidt, M.; Williams, G. J.; Boutet, S.; Pettersson, L. G. M.; Bogan, M. J.; Nilsson, A. *Nature* **2014**, *510*, 381–384.
- (131) Laksmono, H.; McQueen, T. A.; Sellberg, J. A.; Loh, N. D.; Huang, C.; Schlesinger, D.; Sierra, R. G.; Hampton, C. Y.; Nordlund, D.; Beyre, M.; Martin, A. V.; Barty, A.; Seibert, M. M.; Messerschmidt, M.; Williams, G. J.; Boutet, S.; Amann-Winkel, K.; Loerting, T.; Pettersson, L. G. M.; Bogan, M. J.; Nilsson, A. *J. Phys. Chem. Lett.* **2015**, *6*, 2826–2832.
- (132) Hansen, P. L.; Wagner, J. B.; Helveg, S.; Rostrup-Nielsen, J. R.; Clausen, B. S.; Topsøe, H. *Science* **2002**, *295*, 2053–2055.
- (133) Bahn, S.; Jacobsen, K. W. *Comput. Sci. Eng.* **2002**, *4*, 56–66.
- (134) Humphrey, W.; Dalke, A.; Schulten, K. *J. Mol. Graphics* **1996**, *14*, 33–38.
- (135) Lechner, W.; Dellago, C. *J. Chem. Phys.* **2008**, *129*, 114707.
- (136) MATLAB, version 8.3.0.532 (R2014a); The MathWorks Inc.: Natick, MA, 2014.
- (137) Dien, H.; Deane, C. M.; Knapp, B. *J. Comput. Chem.* **2014**, *35*, 1528–1531.